Spatial Resolution of the Nose Cone Prototype Drift Chamber

G.P.Gilfoyle[a], S.Levy[a], and M.Mestayer[b]

[a]University of Richmond, Richmond, VA, USA
[b]CEBAF, Newport News, VA, USA

1. Introduction

The CEBAF Large Acceptance Spectrometer (CLAS) is designed to have a momentum resolution in the range $\delta p/p \approx 0.5 - 1.0\%$ and an angular resolution of about 1.0 $mrad$[1]. Three regions of drift chambers will provide the information necessary to reconstruct the trajectories of the scattered particles. To reach the desired momentum resolution the distance of closest approach of a track to a sense wire must be determined within a resolution of about 200 μm. A prototype of the CLAS drift chambers (referred to here as the nose cone prototype) has been built to serve as a test platform for the construction and operation of the full detector and to act as an early warning of aging problems. In this CLAS Note we discuss some of the techniques we have developed to measure the spatial resolution of the nose cone prototype and present our results.

The outline of this Note is as follows. The nose cone prototype is described first. We then discuss two methods for measuring the spatial resolution of the detector and the contribution made by our fitting procedure in determining the resolution. At the same time we present our results for the resolution of the nose cone prototype.

2. The Nose Cone Prototype

This study was performed with the Region-3, 'nose cone', prototype chamber in a cosmic-ray telescope (see Figure 1 below for a schematic drawing). The prototype reproduces the most-forward-angle portion of the Region 3 drift chambers and contains 192 sense wires, instead of the 2304 sense wires of an actual chamber, but in other aspects of construction and on-board instrumentation is the same. The chamber has a hexagonal wire arrangement, with sense wires grouped into two six-layer superlayers. For the work described here a 50:50 mixture of Argon-Ethane was used. The chamber was operated with sense, field, and guard wires set at $+1800\ V$, $-900\ V$, and $+643\ V$, respectively. The leakage currents for the sense, field, and guards wires were all in the range $8 - 15\ nA$ during the entire run.

The sense wires were amplified in two stages with a gain of 20 $mV/\mu A$. The amplified signal was discriminated with a Philips 706 module with a threshold set to 10 mV. Subsequent analysis of the data (to be presented in a later CLAS Note) leads us to estimate that this threshold corresponds to a minimum detectable signal of three electrons. The discriminator output provided a stop to one of the channels of a LeCroy 2228 TDC module.

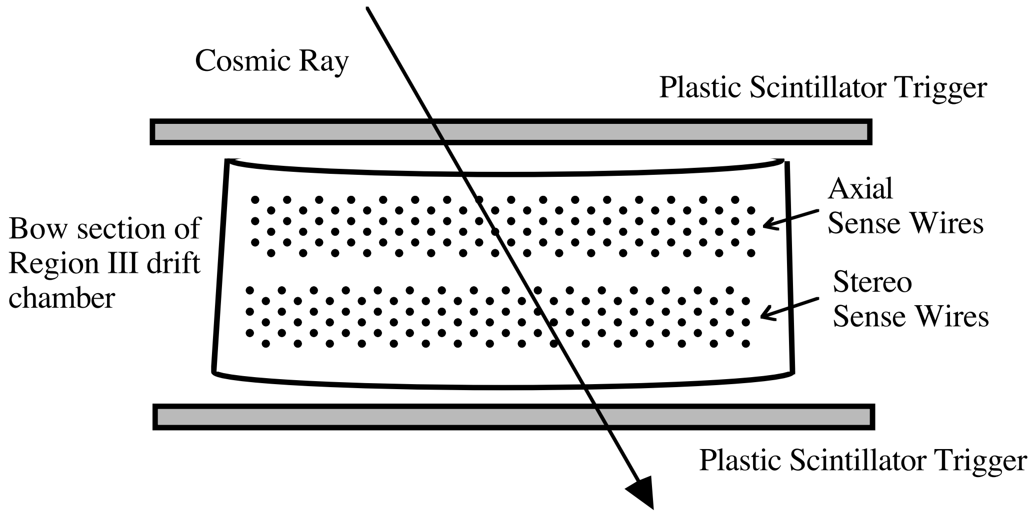

Figure 1 Schematic drawing of the nose cone prototype drift chamber.

Cosmic rays were detected in the chamber with a telescope consisting of two pairs of plastic scintillators placed above and below the chamber. Time jitter occurred in the start signal with a range of $1 - 2\ ns$. This effect was due to variation for different tracks of the propagation time in the scintillator and the time-of-flight of the cosmic ray between the chamber and the scintillators. Data acquisition was done with an array of CAMAC modules and the computer code TRACK[1] running on a MicroVax computer. We fit cosmic ray tracks by minimizing the residual between the calculated distance-of-closest-approach (D) of the fitted track to a wire with the distance from the wire as generated from its drift time (T) alone.

3. The χ^2 Probability Distribution Function

The average resolution for all wires in the chamber can be determined from the distribution of χ^2 from tracks produced by cosmic rays. When a cosmic ray passed through each super-layer in the prototype it left behind a trail of ionized gas molecules in the drift chamber and creates a burst of light in the plastic scintillators. A start signal for the time-to-digital converter (TDC) was formed from a coincidence between the two scintillator signals. In the drift chamber the ions near each sense wire drift into the positive-voltage sense wires and produce a signal used as a stop for a time-to-digital converter (TDC). These measured drift times were then converted into distance-of-closest-approach using a functional form described elsewhere[3]. The position of the track at each sense-wire layer is then fitted with a straight line by minimizing the unnormalized χ_u^2 defined as

$$\chi_u^2 = \sum_{i=1}^{6} (x_i - \mu_i)^2 \tag{1}$$

where the sum is over the six wires in each superlayer, the x_i are the measured track positions extracted from the drift time and the μ_i are the fitted track positions. We use the term unnormalized to describe this quantity since one typically divides each term in Equation 1 by the variance of the measurement, σ_i^2. In our case this variance is unknown and it is the quantity we want to measure.

We expect the measured track positions (the x_i's) to be independent Gaussian-distributed variables so the properly normalized χ^2 probability distribution function (pdf) for n degrees of freedom is

$$f(z;n) = \frac{z^{\frac{n}{2}-1} e^{-z/2}}{2^{n/2}\Gamma(n/2)} \tag{2}$$

where

$$z = \frac{\sum^n (x_i - \mu_i)^2}{\sigma_i^2} \qquad .$$

Since σ_i is the quantity missing from the unnormalized χ^2 defined in Equation 1 we expect the probability distribution function of χ_u^2 to be

$$f(y;n) = \frac{y^{\frac{n}{2}-1} e^{-y/2\sigma^2}}{(2\sigma^2)^{n/2}\Gamma(n/2)} \tag{3}$$

where we have made the change of variable

$$y = \chi_u^2 = \sigma^2 z \qquad . \tag{4}$$

We have assumed the spatial resolution is the same for each wire so $\sigma_i = \sigma$, a constant.

A histogram of the unnormalized χ^2 for the data set collected during a four-day period starting on September 14, 1995 is shown in Figure 2. The distribution shows a sharp peak at about 0.001 cm^2 and drops off sharply. It reveals an excess of tracks with large χ_u^2 (outliers) due to noise and δ-rays. We have fit the distribution with Equation 3 in the region $0 \le \chi_u^2 \le 0.004$ cm^2 which encompasses 90% of the real tracks. The solid line shows the fit. We find a resolution of $\sigma = 229 \pm 2$ μm for the resolution.

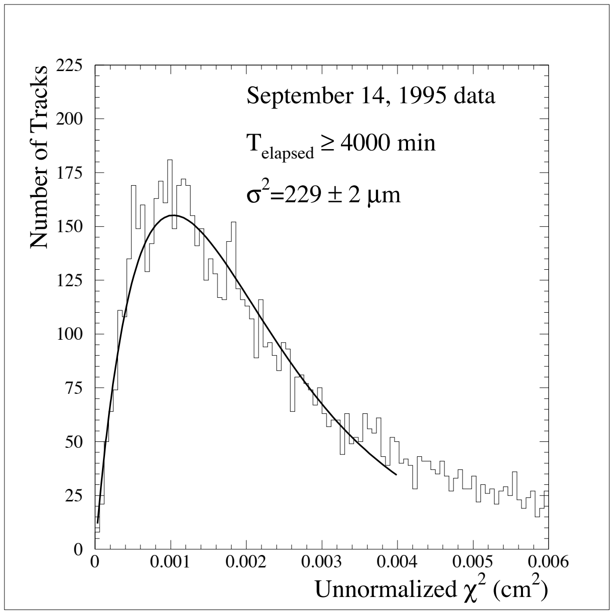

Figure 2. The distribution of the unnormalized χ^2 for the September 14, 1995 run.

There are several advantages to determining the resolution in this manner. The histogram of χ^2_u is simple to extract and the fit results are easy to interpret. The sharpness of the peak in the distribution provides an excellent indicator of the resolution of the drift chamber and would be a useful monitoring tool. The distribution also reveals the region of 'good' tracks and where the data are dominated by 'outliers'. The main disadvantage of the χ^2_u probability distribution is that it characterizes the entire track. One must examine different observables to monitor other aspects of detector performance like the resolution as a function of D or the rate of cross-talk.

4. The Excluded Layer Residual

An alternative measure of the drift chamber resolution is the excluded layer residual. One of the six layers in the super layer is left out of the least-squares fit to the remaining five layers and the difference between the distance-of-closest-approach extracted from the drift time is subtracted from the distance-of-closest-approach to the wire determined from the fitted line. The width of this distribution can then be determined by calculating the root-mean-square deviation or by fitting the residual distribution with a Gaussian curve. The results of such a fit are shown in Figure 3 for the data set discussed above. The layer excluded form the fit is the third layer in the superlayer. The range of the fit is restricted to the region within 500 μm of the origin. This restriction will exclude wires that have large-magnitude residuals ('outliers') that are due to noise or δ-rays. The range of the fit still encompasses over 97% of the 'good' hits.

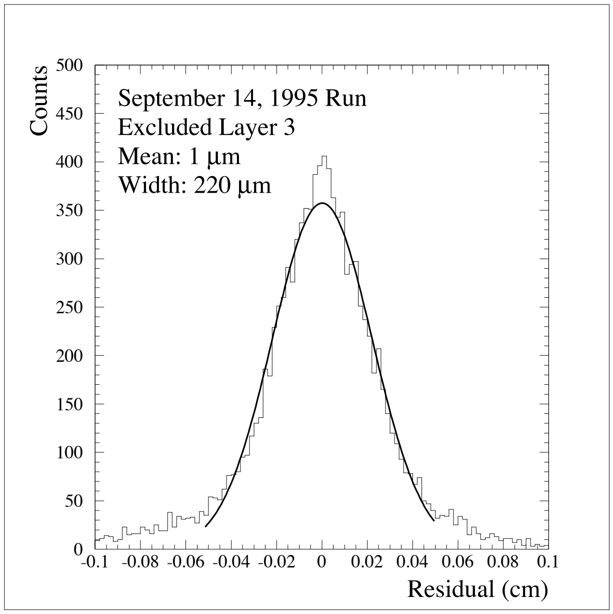

Figure 3. The distribution of the residual in the excluded layer for the September 14, 1995 run.

The width of this distribution contains contributions from the true spatial resolution and a second component due to the extrapolation of the fit from the remaining layers so

$$\sigma^2_{total} = \sigma^2_{fit} + \sigma^2_{spatial} \qquad .$$

The estimated variance of the fit contribution of an interpolated (or extrapolated) value of D at point x is [4]

$$(D - D_{true})^2 = \frac{1}{S_1} + \frac{S_1}{F}\left(x - \frac{S_x}{S_1}\right)^2 \tag{5}$$

where

$$F = S_1 S_{xx} - S_x^2 \tag{6}$$

and

$$S_1 = \sum \frac{1}{\sigma_i^2} \quad S_x = \sum \frac{x_i}{\sigma_i^2} \quad S_{xx} = \sum \frac{x_i^2}{\sigma_i^2} \tag{7}$$

The σ_i in Equations 6-7 is the spatial resolution of each layer which we have treated as a constant. We have assumed that this value is constant for all wires and used the value of $229 \pm 2\ \mu m$ we found in our analysis of the χ^2_u probability distribution function. The dependence of the variance on position is displayed in Figure 4. The curve is from Equation 5 and the open circles represent the wire positions in the axial superlayer. We typically exclude layer three from the fit with this method which has a standard deviation of 109 μm that is added in quadrature to the spatial resolution.

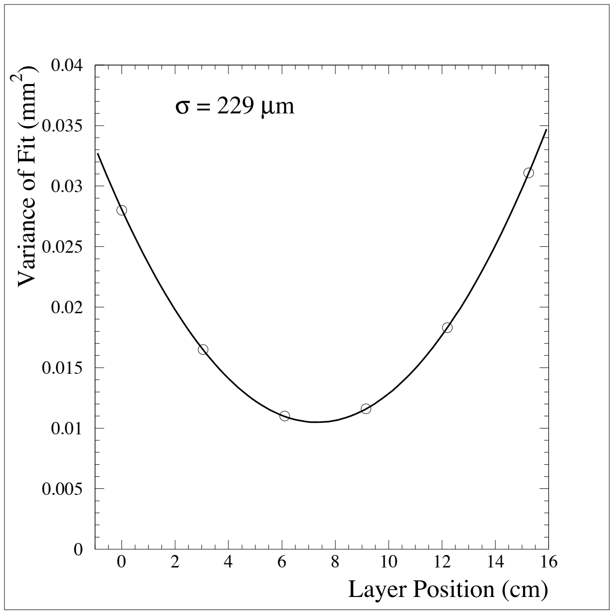

Figure 4. The variance associated with the straight-line fit to the cosmic rays tracks in the nose cone prototype. The open circles represent the fit variance at the positions of the wires in each superlayer. The origin is placed at the position of the first layer in the superlayer.

We find that the width of the excluded layer residual (that contains the components of the spatial and fit resolutions) in the region within 500 μm of the origin is 220 μm so the true spatial resolution is 190 μm. We note here that this result differs from the resolution determined from the χ^2 probability function by about 15%. However, the spatial resolution determined from the excluded layer residual is sensitive to the choice of fitting region and includes hits from large-χ^2_u that are avoided in χ^2_u pdf. The resolution extracted from the χ^2_u p.d.f. is also sensitive to the choice of the cutoff described in Section 3.

We have also explored the dependence of the excluded layer resolution on the distance-of-closest-approach. The distribution of the excluded layer residual was generated for a range of D and the distribution fitted to determine the width. Our results are shown in Figure 5. The resolution is poor near the sense wire where discrete ionization effects are large and also near the field wire (large D) for the same reason. The solid curve in the Figure 5 is a calculation of the expected resolution without including the effects of the discrete ionization. The contributions to this resolution are from diffusion which for argon-ethane can be parameterized by [1]

$$\sigma_{diffusion} = d\sqrt{D} \tag{9}$$

where $d = 0.01\ cm^{-1/2}$. The other contributions to the resolution are 63 μm from jitter in the T_o calibration, 75 μm from machining imperfections, and 50 μm from the uncertainty of the propagation time of the light in the plastic scintillator. These contributions were added in quadrature to obtain the curve in Figure 5. We note that in the central region of the cell we are close to the limit we expect for the spatial resolution.

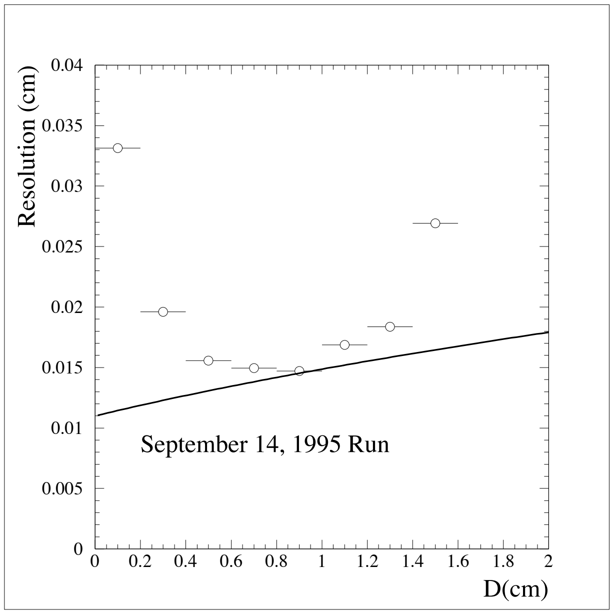

Figure 5. The resolution as a function of distance of closest approach.

References

[1] 'Conceptual Design Report - Basic Experimental Equipment', CEBAF, April 13, 1990.

[2] S.Zhou and R.T.Edwards, 'The CLAS Drift Chamber Track System', CLAS-NOTE-91-001.

[3] E.Burtin, G.P.Gilfoyle, M.V.Kossov, M.D.Mestayer, and L.Y.Murphy, 'Drift Velocity Calibration of the CLAS Drift Chambers', CLAS-NOTE-95-022.

[4] Particle Data Group (1994): Review of particle Properties, Physical Reveiw, D50, 3-I.